GaSb-based Interband Cascade Lasers with Advanced Waveguides Operating near 3.3 and 3.4 µm

Jeremy A. Massengale[a,b], Yixuan Shen[a], Rui Q. Yang*[a], Tetsuya D. Mishima[b], and Michael B. Santos[b]

[a]School of Electrical and Computer Engineering, University of Oklahoma, Norman, OK USA 73019
[b]Homer L. Dodge Department of Physics and Astronomy, University of Oklahoma, Norman, OK USA 73019

ABSTRACT

We report the first implementation of an advanced waveguide structure, consisting of GaSb separate confinement layers (SCLs), n-doped InAs/AlSb superlattice (SL) intermediate cladding layers, and n^+-doped $InAs_{0.91}Sb_{0.09}$ plasmon enhanced cladding layers for GaSb-based interband cascade lasers (ICLs) with lasing wavelengths at 3.3 and 3.4 µm. This advanced waveguide structure is intended to improve the optical confinement and the overall thermal conductivity of these ICLs. A room temperature (RT) threshold current density (J_{th}) as low as 176.9 A/cm^2 for a broad area (BA) device emitting at 3.28 µm was measured with the pulsed operation extending up to 390 K. A second ICL emitting at 3.42 µm exhibited a RT pulsed J_{th} of 195.6 A/cm^2. The ICLs tested here had characteristic temperatures (T_o) of nearly 60 K, which is the highest among RT ICLs with similar lasing wavelengths, suggesting advantages of the advanced waveguide in these devices.

Keywords: interband cascade laser, quantum wells, mid-infrared, semiconductor lasers, type-II heterostructures, semiconductor waveguide, III-V materials

1. INTRODUCTION

Interband cascade lasers (ICLs)[1] based on a type-II quantum well (QW) active region have attracted much interest over the years, in large part due to their low power consumption. Their operation hinges on two key features: interband transitions in type-II quantum wells and a cascade configuration, which enhances the total gain (per current density)[1-5] and was first developed for quantum cascade lasers (QCLs).[6] However, the ICL stands apart from the QCL in that its interband transition nature makes it immune to phonon scattering, a key loss mechanism for the QCL, which allows the ICL to lase at a much lower threshold current density (J_{th}). These features of the ICL are ideal for a host of practical applications in the mid-infrared (MIR) including gas/chemical sensing, imaging, industrial process control, and free-space optical communication.[7-10] The GaSb-based ICLs have demonstrated efficient room temperature (RT) operation in the 3-6 µm range but exhibited performance below their InAs-based counterparts beyond 6 µm due partially to limited effort and the difficulties associated with the waveguide traditionally used.[4,5] The typical waveguide used in a GaSb-based ICL consists of two Te-doped GaSb separate confinement layers (SCLs) surrounding the cascade active region, wrapped by two n-doped InAs/AlSb superlattice (SL) cladding layers, which have a low thermal conductivity and a small contrast in refractive index with the cascade region. The InAs-based ICLs have utilized a heavily n^+-doped InAs plasmon enhanced cladding layer, instead of the InAs/AlSb SL, to improve the optical confinement and the overall thermal conductivity of the device[11-17], resulting in the wavelength coverage of ICLs extending to 11.2 µm. For InAs-based ICLs operating near 4.6 µm, it was later shown that an advanced waveguide structure which combined a relatively thin InAs/AlSb SL intermediate cladding layer with the n^+-doped InAs plasmon cladding, enabled enhanced device performance by reducing the free-carrier loss and yielding improved optical confinement within the cascade active region[18]. This advanced waveguide was later shown to improve performance in long wavelength InAs-based ICLs emitting between 10-13 µm[19-20] and was also explored in GaSb-based ICLs operating between 3.8 to 6.1 µm,[21-22] where the plasmon enhanced cladding layer in the latter is composed of n^+-doped $InAs_{0.91}Sb_{0.09}$. Here we report an investigation of GaSb-based ICLs which incorporate this advanced waveguide structure and are tailored to emit near 3.3 and 3.4 µm at RT. The continuous wave (cw) and pulsed performance of these broad area (BA) ICLs display similar performance to other GaSb-based ICLs which utilize the conventional waveguide and emit near a similar wavelength.

*Rui.q.Yang@ou.edu

2. DESIGN, GROWTH, AND FABRICATION

Two GaSb-based ICL wafers were grown with designs utilizing the advanced waveguide structure. Both ICL wafers have 6 cascade stages (N_c) where each W-QW active region consists of an identical layer sequence of AlSb/InAs/$Ga_{0.6}In_{0.4}Sb$/InAs/AlSb for a targeted lasing wavelength near 3.3 µm at RT. The primary difference between the two ICL wafers stems from the variation in the SCL layer thickness. The first ICL structure (Y082L) has GaSb SCLs doped with Te to a level of 2.7×10^{17} cm^{-3} each with a thickness of 2100 Å, while the second ICL structure (Y083L) incorporates the same Te-doped GaSb SCLs but with the thickness increased to 3000 Å. Both include 1 µm thick (bottom) and 0.7 µm thick (top) n^+-doped $InAs_{0.91}Sb_{0.09}$ plasmon cladding layers with a doping level of 3.2×10^{19} cm^{-3} and 0.75 µm (bottom and top) n-doped (1.5×10^{17} cm^{-3}) InAs/AlSb SL cladding layers. Figures 1a and 1b show the calculated optical modal profile and refractive index for these two ICL wafers. To calculate characteristics at RT, the waveguide simulation was generated using the measured pulsed wavelength at 300 K, which was λ = 3.28 µm for Y082L and λ = 3.42 µm for Y083L. Several estimated parameters are shown in the figures, including the optical confinement factor (Γ), the internal loss due to free carrier absorption (α_i), the threshold gain (G_{th}), and the effective refractive index (n_{eff}) of the waveguide. Note that the estimated optical confinement factor decreases from approximately 20.7% in Y082L to 19.1% in Y083L due to the increased thickness of the SCLs. On the other hand, the increase in the SCL thickness in Y083L leads to predicted reductions in the free carrier absorption loss of nearly 31% and the required threshold gain of about 7%.

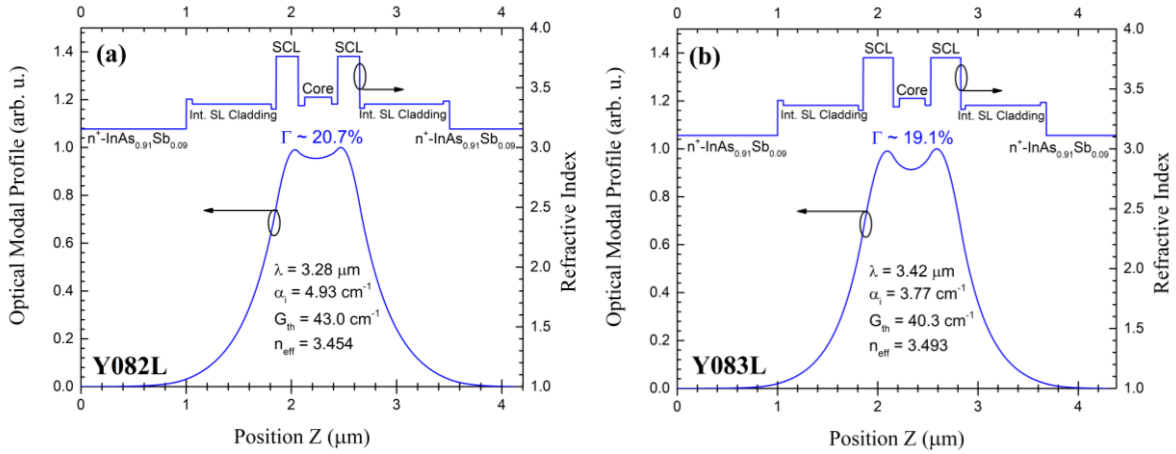

Figure 1. The calculated optical modal profile and refractive index for (a) Y082L and (b) Y083L. Listed in the plots are the optical confinement factor (Γ), the internal loss due to free carrier absorption (α_i), the threshold gain (G_{th}), and the effective refractive index (n_{eff}).

The two six-stage GaSb-based ICL wafers were grown by molecular beam epitaxy (MBE) using a Veeco GenXplor with As and Sb supplied by valved cracking sources. The crystalline quality of the grown ICL wafers was analyzed using x-ray diffraction (XRD) and the surface morphology was characterized by differential-interference-contrast microscopy (DIC). From the DIC images, typical oval hillock defects were observed – common to III-V ICL growth, but with little background surface roughness. The average surface defect density of Y082L was 1.4×10^4 cm^{-2}, while that of Y083L was 6.8×10^3 cm^{-2}, which are within acceptable limits for reasonable device performance. From the XRD measurements, symmetric scans normal to the (004) planes indicate certain deviations from the intended design as shown in Figure 2. Between both ICL wafers, an average tensile strain for the SL cladding of 0.13% in the growth direction (biaxial compressive strain) was observed, where the average substrate/SL zero-order peak separation was

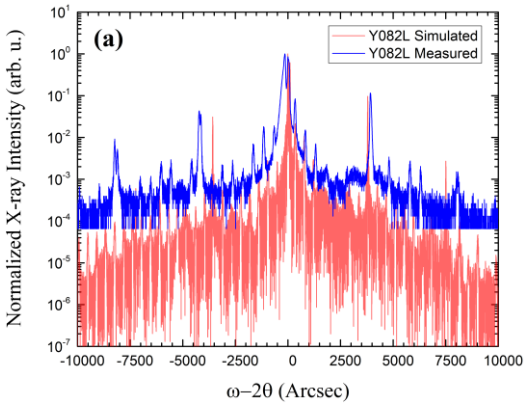

Figure 2. The experimentally measured XRD spectrum (blue) along with the simulated spectrum (red) for Y082L.

approximately 159 arcsec. The analysis of the XRD spectrum showed that on average, the InAs/AlSb SL cladding was about 8.3% thinner than expected, while the cascade region was 13% thinner than expected, indicating variance in the group III growth rates. Despite these structural deviations, devices made from these ICL wafers exhibited reasonable lasing performance in both cw and pulsed modes, as discussed in Section 3.

The grown ICL wafers were fabricated into 100-µm-wide (e.g. Y082LBA1-3F and Y083LBA1-3G) and 150-µm-wide (e.g. Y082LBA1-3H and Y083LBA1-3E) broad area (BA) mesas using standard UV contact photolithography and wet chemical etching. The wafers were left unthinned and cleaved into approximately 3-mm-long (and 1.5-mm-long) laser bars without facet coating, which were mounted epi-side up on copper heat sinks for testing.

3. EXPERIMENTAL RESULTS

Figure 3 depicts the measured threshold voltage (V_{th}) and threshold current density (J_{th}) values as a function of temperature for two representative devices from the first ICL wafer, Y082LBA1-3F and Y082LBA1-3H. Also shown are the specific thermal resistance (R_{th}) and the characteristic temperature (T_o), which was determined from the pulsed measurements. In cw mode, Y082LBA1-3F lased at 80 K with an emission wavelength of λ = 2.89 µm, a J_{th} = 10.5 A/cm^2, and a V_{th} = 7.4 V. Y082LBA1-3F went on to operate up to 242 K in cw mode, with an emission wavelength of λ = 3.25 µm and a J_{th} of 165 A/cm^2. Y082LBA1-3H exhibited similar 80 K performance and operated up to a maximum cw temperature of 225 K with an emission wavelength of λ = 3.21 µm and a J_{th} of 106.9 A/cm^2. The cw operating temperature difference between the two devices is likely due to the increased thermal load in device H stemming from the wider laser ridge, which is reflected by their difference in the specific thermal resistance.

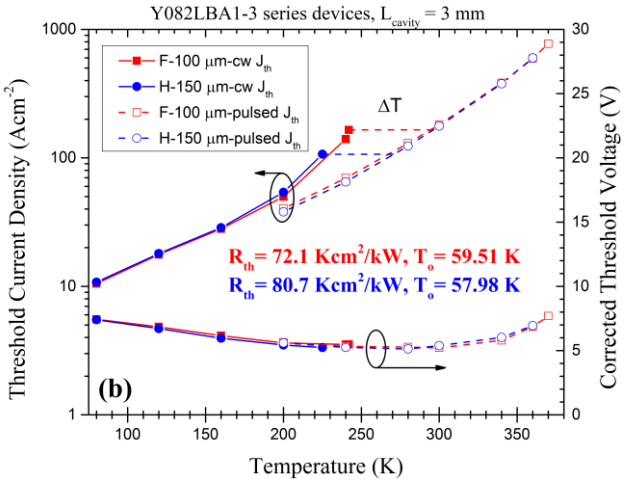

Figure 3. The J_{th} and V_{th} as a function of temperature for two representative devices from ICL wafer Y082L with different laser ridge widths in both cw and pulsed modes. Included are the calculated R_{th} and T_o values.

Figures 4a and 4b show the cw current-voltage-light (IVL) characteristics of devices Y082LBA1-3F and Y082LBA1-3H, respectively. Y082LBA1-3F reached a source-limited cw output power at 80 K of 121.5 mW/facet at an injection current of 500 mA with an extracted external quantum efficiency (EQE) of 131%, indicating the cascaded emission of photons in the ICL, and dropped to 27% at 240 K with a cw output power of 4.4 mW/facet. Y082LBA1-3H showed similar performance, with a source-limited cw output power at 80 K of 116 mW/facet and a corresponding EQE of 147%, dropping to 32% at 225 K with a cw output power of 1.9 mW/facet. In pulsed operation, the Y082LBA1-3F and Y082LBA1-3H devices were able to lase up to 370 K with a J_{th} = 773 A/cm^2 and 360 K with a J_{th} = 600 A/cm^2, respectively, as shown in Figure 5. Another device with a 1.5 mm cavity length and a 100 µm wide ridge, Y082BA1-1C, was operated up to 390 K and then damaged with a high pulsed current. Y082LBA1-3F lased in pulsed mode at RT with an emission wavelength of λ = 3.28 µm and a J_{th} = 181.3 A/cm^2, while Y082LBA1-3H lased at a similar wavelength with a J_{th} = 176.9 A/cm^2. This is somewhat similar to a 5-stage GaSb-based ICL which utilized the traditional waveguide and exhibited RT lasing at λ = 3.6 µm with a J_{th} = 134 A/cm^2.[23] As ref. [23] points out, the threshold tends to increase at even shorter wavelengths, rising above 200 A/cm^2 for devices emitting below 3.1 µm. However, the threshold voltages from devices made from Y082L were relatively high (>5 V) as illustrated in Fig. 3, suggesting unsmooth carrier transport. This might be caused by substantial deviations in layer thicknesses from the design. Nevertheless, these ICLs were able to lase in pulsed mode at high temperatures (up to 390 K) with T_o values close to 60 K as shown in Fig. 3, which is the highest among RT ICLs with similar lasing wavelengths. These preliminary results are very encouraging

considering that these ICL wafers were the first growth trial after repairing the MBE system (which was partially damaged by a severe storm).

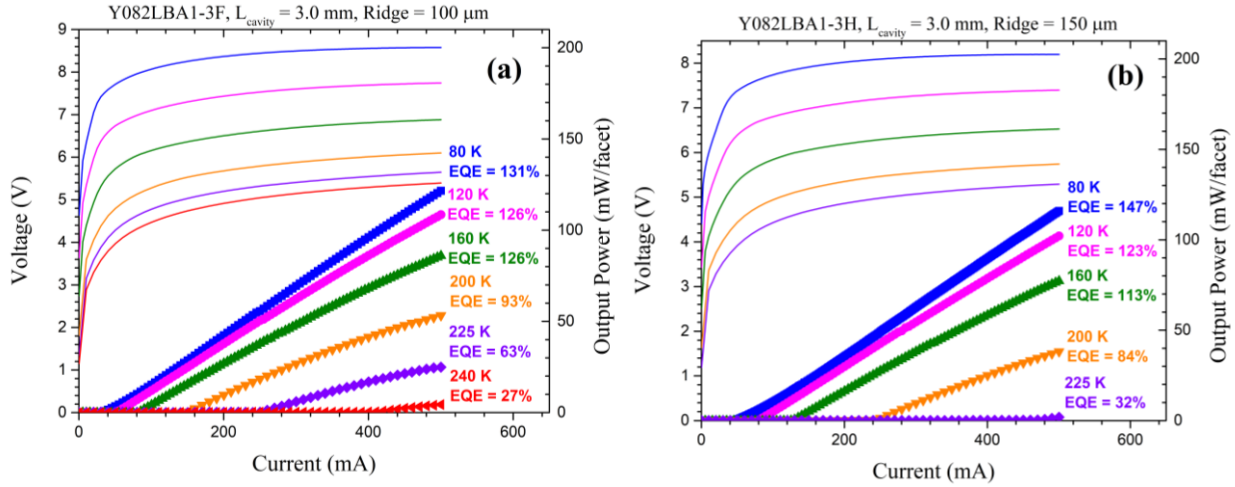

Figure 4. CW IVL characteristics for Y082LBA1-3F (a) and Y082LBA1-3H (b) from 80 K to their maximum operating temperatures of 240 K and 225 K, respectively. Also shown are the extracted external quantum efficiency values (EQE).

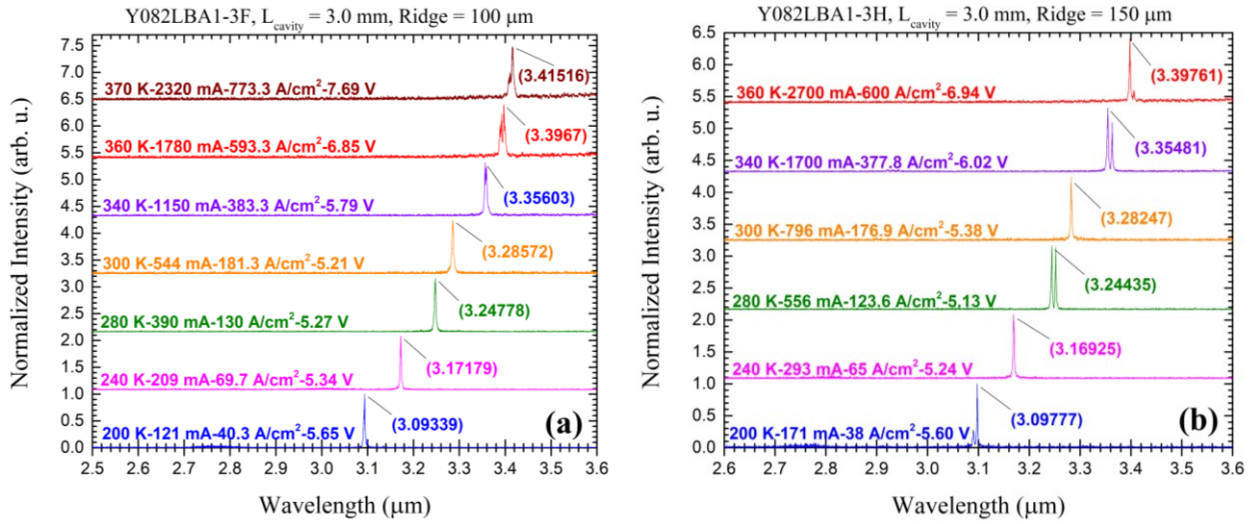

Figure 5. Normalized spectra under pulsed excitation for (a) Y082LBA1-3F and (b) Y082LBA1-3H. Shown in the plot are the threshold current, threshold current density, threshold voltage, and emission wavelength at each temperature step.

Two representative devices from the second ICL wafer, Y083LBA1-3G and Y083LBA1-3E were able to lase in both cw and pulsed modes as shown in Figure 6. In cw mode at 80 K, Y083LBA1-3G lased at λ = 3 µm with a J_{th} = 10.4 A/cm^2 and a V_{th} = 9.14 V, which is a higher threshold voltage than that of Y082LAB1-3F. This device went on to operate up to 228 K in cw mode with an emission wavelength of λ = 3.35 µm and a J_{th} = 120 A/cm^2. As before, the companion device (Y083LBA1-3E) exhibited similar performance at 80 K, with a J_{th} = 11.2 A/cm^2 and was able to lase up to 210 K in cw mode, with emission near λ = 3.31 µm and a J_{th} = 87 A/cm^2.

Figures 7a and 7b show the cw IVL characteristics of devices Y083LBA1-3G and Y083LBA1-3E, respectively, where damage to the devices was avoided by limiting the injection current to 400 mA at lower temperatures. Under this restriction, Y083LBA1-3G reached a peak cw output power at 80 K of 109.1 mW/facet with an extracted external quantum efficiency (EQE) of 153%. Compared to a similar injection current for Y082LBA1-3F (96.1 mW/facet at 400 mA), the output at 80 K from Y083LBA1-3F was about 13.5% larger. The output power dropped to 1.5 mW/facet, with an EQE of 21%, at its maximum cw operating temperature of 228 K. At a comparable cw operating temperature of 225 K, the output from Y083LBA1-3G (8.7 mW/facet) was much lower than that of Y082LAB1-3F (24.9 mW/facet) under an injection current of 500 mA. This may be due partially to the increased heating with the higher threshold voltage and the thicker SCL as it may slightly reduce the efficiency of the heat extraction from the active region. Y083LBA1-3E exhibited similar performance, with an 80 K EQE = 136% and a maximum cw output power of 90.6 mW/facet, which is again quite comparable to the equivalent output of Y082LBA1-3H (89.7 mW/facet) under a similar injection current. The output fell to 5.7 mW/facet at 210 K with an EQE = 36%. Under comparable injection currents at 200 K, the output of Y083LBA1-3E was 22.8 mW/facet while that of Y082LBA1-3H was about 68% larger at 38.2 mW/facet, again indicating reduced performance possibly due to the increased thermal load in devices from Y083L. This is also supported by comparison of both devices from Y083L at 200 K. Y083LBA1-3G showed an output of 39.4 mW/facet at 200 K, indicating the reduced performance seen in Y083LBA1-3E is associated with heating in the QW active region due to the wider laser ridge compared with Y083LBA1-3G.

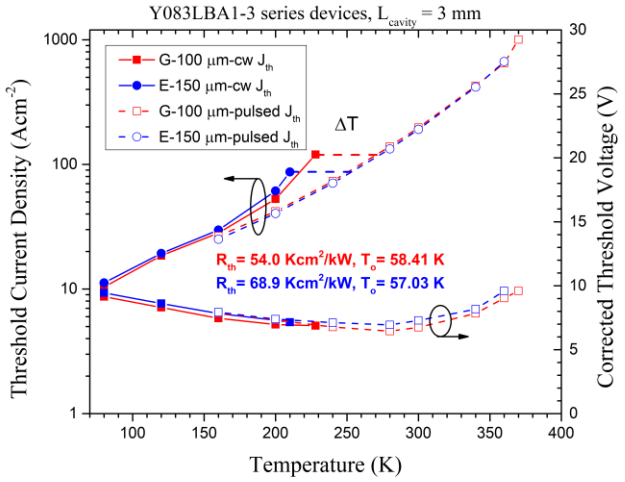

Figure 6. The J_{th} and V_{th} as a function of temperature for two representative devices from ICL wafer Y083L with different laser ridge widths in both cw and pulsed modes. Included are the calculated R_{th} and T_o values.

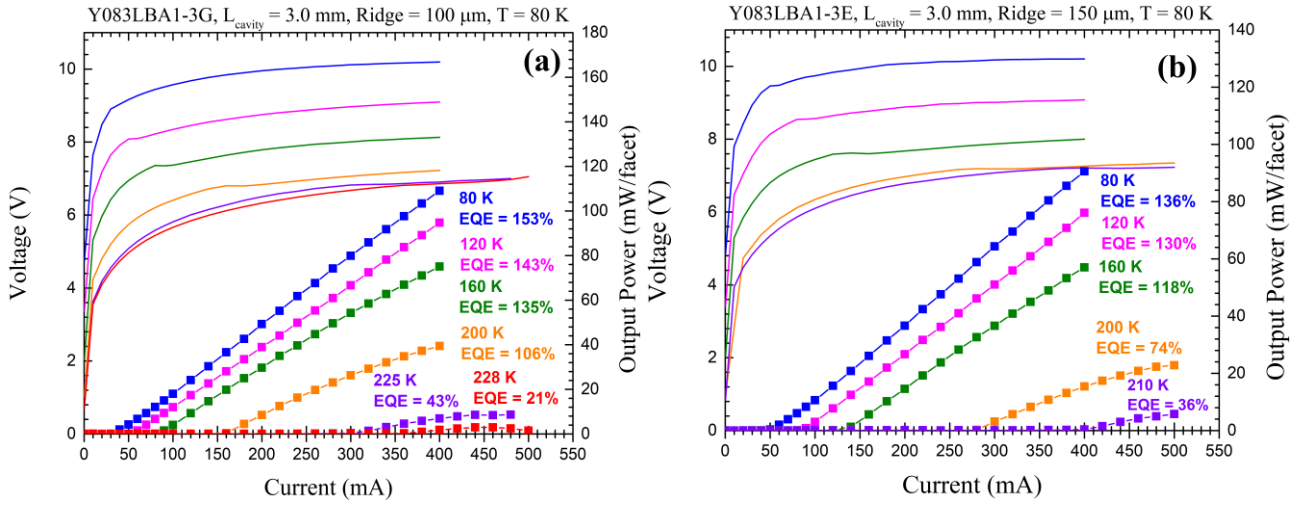

Figure 7. CW IVL characteristics for (a) Y083LBA1-3G and (b) Y083LBA1-3E from 80 K to their maximum operating temperatures of 228 K and 210 K, respectively. Also shown are the extracted external quantum efficiency values (EQE).

In pulsed operation devices Y083LBA1-3G and Y083LBA1-3E were able to lase up to 370 K with a J_{th} = 1003.3 A/cm^2 and 360 K with a J_{th} = 668.9 A/cm^2, respectively, as shown in Figure 8. No device from this ICL wafer was taken to failure but considering the increased heat load with the higher threshold voltage, these devices could fail at slightly

reduced temperatures compared with those made from Y082L. Y083LBA1-3G lased at RT with an emission wavelength of λ = 3.42 μm and a slightly larger J_{th} = 197.3 A/cm^2 compared to Y082LBA1-3F. Y083LBA1-3E lased at a similar wavelength with a J_{th} = 195.6 A/cm^2.

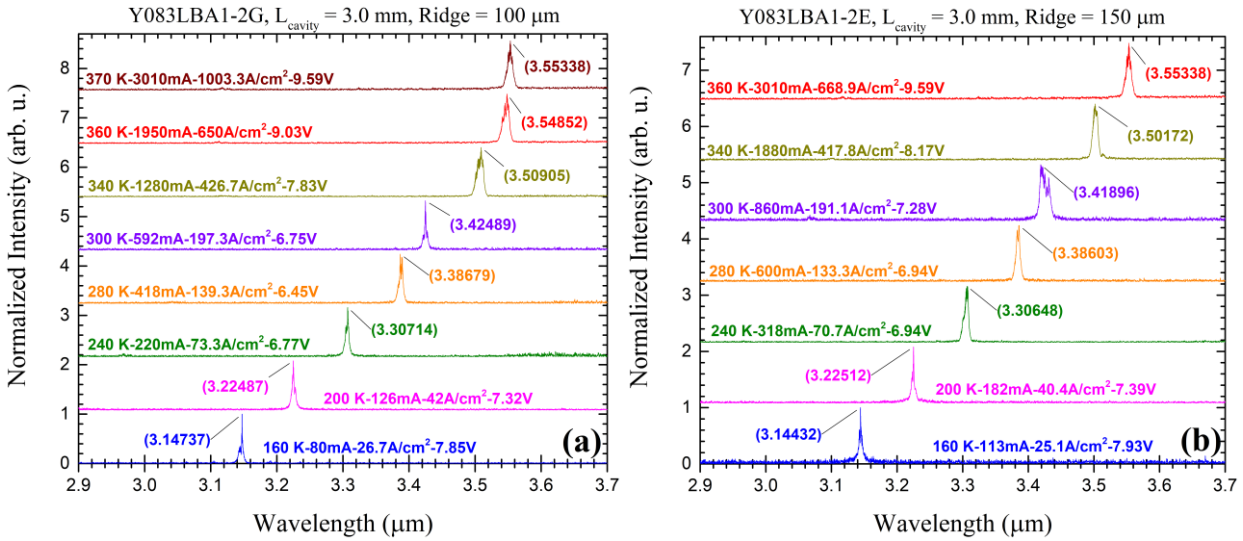

Figure 8. Normalized spectra under pulsed excitation for (a) Y083LBA1-3G and (b) Y083LBA1-3E. Shown in the plot are the threshold current, threshold current density, threshold voltage, and emission wavelength at each temperature step.

Devices made from Y082L and Y083L showed similar performance between 80 K and their maximum pulsed operating temperatures, with devices from Y083L generally performing slightly worse overall. Though the increased thickness of the SCL reduces the optical confinement within the QW active region for devices from Y083L, based on simulation results in Fig. 1 there should be trade-off benefits in reductions of the threshold gain and free-carrier absorption loss. In practice, however, the trade-offs do not seem to aid the performance of devices from Y083L. This might be due to some uncertainties related to variations among the ICL structures during the MBE growth and device fabrication processes considering that the V_{th} in devices made from Y083L was larger than that in devices from Y082L.

4. SUMMARY

To summarize, two six-stage ICL wafers were grown on GaSb substrates, both of which incorporated waveguides with Te-doped GaSb SCLs, n-doped InAs/AlSb SL intermediate cladding layers, and n^+-doped $InAs_{0.91}Sb_{0.09}$ plasmon enhanced cladding layers. This advanced waveguide structure has been shown to enhance the performance of InAs-based ICLs operating between 4-13 μm and GaSb-based ICLs operating between 4-6 μm and was implemented here for the first time in GaSb-based ICLs designed to lase at wavelengths shorter than 3.5 μm at RT. Threshold current density results that are comparable to state-of-the-art GaSb-based ICLs operating at 3.6 μm were observed, with measured characteristic temperature values that are the highest among ICLs around RT and emitting at similar wavelengths. We believe that with further design and growth iterations, GaSb-based ICLs which utilize the advanced waveguide structure may display enhanced performance between 3-4 μm at room temperature.

Acknowledgements

This work was partially supported by NSF (No. ECCS-1931193) and OCAST (AR21-024).

REFERENCES

[1] R. Q. Yang, "*Infrared laser based on intersubband transitions in quantum wells",* Superlattices Microstruct., **17**, 77 (1995).

[2] R. Q. Yang, "Interband cascade (IC) lasers," in Semiconductor Lasers Fundamentals and Applications, edited by A. Baranov and E. Tournie (Woodhead Publishing, Cambridge, 2013), Chap. 12, pp. 487–513.

[3] J. Koeth, R. Weih, J. Scheuermann, M. Fischer, A. Schade, M. Kamp, and S. Höfling, "Mid infrared DFB interband cascade lasers," Proc. SPIE 10403, 1040308 (2017).

[4] R. Q. Yang, L. Li, W. Huang, S. M. Shazzad Rassel, J. A. Gupta, A. Bezinger, X. Wu, G. Razavipour, and G. C. Aers, "InAs-based interband cascade lasers," IEEE J. Sel. Top. Quantum Electron. 25, 1200108 (2019).

[5] J. R. Meyer, W. W. Bewley, C. L. Canedy, C. S. Kim, M. Kim, C. D. Merritt, and I. Vurgaftman, "The interband cascade laser," Photonics **7**, 75 (2020).

[6] J. Faist, F. Capasso, D. L. Sivco, C. Sirtori, A. L. Hutchinson, A. Y. Cho, "Quantum cascade laser," Science **264**, 553–556 (1994).

[7] I. Vurgaftman, P. Geiser, W. W. Bewley, C. D. Merritt, C. L. Canedy, M. V. Warren, M. Kim, C. S. Kim, and J. R. Meyer, "Sensitive chemical detection with distributed feedback interband Cascade lasers," in Encyclopedia of Analytical Chemistry, edited by R. A. Meyers (Wiley, Chichester, 2016).

[8] J. Scheuermann, P. Kluczynski, K. Siembab, M. Straszewski, J. Kaczmarek, *et al*, "Interband Cascade Laser Arrays for Simultaneous and Selective Analysis of C1–C5 Hydrocarbons in Petrochemical Industry", Applied Spectroscopy **75** (3), 336-342 (2021).

[9] C. S. Goldenstein, R. M. Spearrin, J. B. Jeffries, and R. K. Hanson, "Infrared laser-absorption sensing for combustion gases," Prog. Energy Combust. Sci. **60**, 132–176 (2017).

[10] A. Soibel, M. W. Wright, W. H. Farr, S. A. Keo, C. J. Hill, R. Q. Yang, and H. C. Liu, "Mid-infrared interband cascade laser for free space optical communication", IEEE Photonics Technol. Lett. **22**, 121 (2010).

[11] Z. Tian, R. Q. Yang, T. D. Mishima, M. B. Santos, R. T. Hinkey, M. E. Curtis, and M. B. Johnson, "InAs-based interband cascade lasers near 6 μm," Electron. Lett. **45**, 48 (2009).

[12] Z. Tian, R. Q. Yang, T. D. Mishima, M. B. Santos, and M. B. Johnson, "Plasmon-waveguide interband cascade lasers near 7.5 μm," IEEE Photonics Technol. Lett. **21**, 1588 (2009).

[13] R. T. Hinkey, Z. Tian, R. Q. Yang, T. D. Mishima, and M. B. Santos, "Reflectance spectrum of plasmon waveguide interband cascade lasers and observation of the Berreman effect," J. Appl. Phys. **110**, 043113 (2011).

[14] Z. Tian, L. Li, H. Ye, R.Q. Yang, T.D. Mishima, M.B. Santos, and M.B. Johnson, "InAs-based interband cascade lasers with emission wavelengths at 10.4 μm," *Electron. Lett.* **48**, 113–114 (2012).

[15] R. Q. Yang, L. Li, L. Zhao, Y. Jiang, Z. Tian, H. Ye, R. T. Hinkey, C. Niu, T. D. Mishima, M. B. Santos, J. C. Keay, M. B. Johnson, and K. Mansour, "Recent progress in development of InAs-based interband cascade lasers," Proc. SPIE **8640**, 86400Q (2013).

[16] Lu Li, H. Ye, Y. Jiang, R. Q. Yang, J. C. Keay, T. D. Mishima, M. B. Santos, and M. B. Johnson, *"*MBE-grown long-wavelength interband cascade lasers on InAs substrates*", Journal of Crystal Growth,* **425**, 369 (2015).

[17] M. Dallner, F Hau, S Höfling, M Kamp, "InAs-based interband cascade lasers emitting around 7 μm with threshold current densities below 1 kA/cm^2 at room temperature", Appl. Phys. Lett., **106**, 041108 (2015).

[18] L. Li, Y. Jiang, H. Ye, R. Q. Yang, T. D. Mishima, M. B. Santos, and M. B. Johnson, "Low-threshold InAs-based interband cascade lasers operating at high temperatures," Appl. Phys. Lett. **106**, 251102 (2015).

[19] J. A. Massengale, Y. Shen, R. Q. Yang, S. D. Hawkins, and J. F. Klem, "Long wavelength interband cascade lasers," Appl. Phys. Lett. **120**, 091105 (2022).

[20] J. A. Massengale, Y. Shen, R. Q. Yang, S. D. Hawkins, and J. F. Klem, "Enhanced Performance of InAs-based Interband Cascade Lasers Emitting between 10-13 μm," Semiconductor Science and Technology **38**, 025009 (2022) https://doi.org/10.1088/1361-6641/acac4e.

[21] C. L. Canedy, M. V. Warren, C. D. Merritt, W. W. Bewley, C. S. Kim, M. Kim, I. Vurgaftman, and J. R. Meyer, "Interband cascade lasers with longer wavelengths," Proc. SPIE **10111**, 101110G (2017).

[22] Y. Lin, J. A. Massengale, W. Huang, R. Q. Yang, T. D. Mishima, M. B. Santos, "Examination of the Durability of Interband Cascade Lasers Against Structural Variations", J. Infrared & Millimeter Waves. **39**, 137 (2020).

[23] I. Vurgaftman, R. Weih, M. Kamp, J. R. Meyer, C. L. Canedy, C. S. Kim, M. Kim, W. W. Bewley, C. D. Merritt, J. Abell, "Interband Cascade Lasers," *J. Phys. D: Appl. Phys.* **48** 123001 (2015).